J Infrared Milli Terahz Waves (2012) 33:777–793
DOI 10.1007/s10762-011-9855-9

X-Ray Detected Magnetic Resonance at Sub-THz Frequencies Using a High Power Gyrotron Source

Andrei Rogalev · José Goulon · Gérard Goujon · Fabrice Wilhelm · Isamu Ogawa · Toshitaka Idehara

Received: 17 October 2011 / Accepted: 27 October 2011 /
Published online: 30 November 2011
© Springer Science+Business Media, LLC 2011

Abstract X-ray Detected Magnetic Resonance (XDMR) is a novel spectroscopy which makes use of X-ray Magnetic Circular Dichroism (XMCD) to probe the resonant precession of local magnetization components in a strong microwave pump field. In Sections 1 and 2, we briefly review the conceptual bases of XDMR and the potential interest of increasing the pumping frequency up to the THz frequency range. In Sections 3–5, we discuss the feasibility of such challenging experiments. Starting from a comparison of experiments carried out either in the *transverse* (TRD) or *longitudinal* (LOD) detection geometries, we show that XDMR measurements at sub-THz frequencies require a substantial increase in pumping power: this is where a gyrotron source looks most appropriate. It is the aim of this paper to discuss how to conduct such experiments, emphasis being laid on feasibility tests recently carried out at the ESRF using a refurbished version of Gyrotron FU-II built at the FIR-FU. In this context, we propose a new detection scheme of sub-THz XDMR spectra based on the concept of *frequency-mixing* in LOD geometry.

Keywords X-ray Detected Magnetic Resonance (XDMR) · X-ray Magnetic Circular Dichroism (XMCD) · Ferromagnetic Resonance (FMR) · Gyrotron

A. Rogalev · J. Goulon (✉) · G. Goujon · F. Wilhelm
European Synchrotron Radiation Facility, B.P. 220, 38043, Grenoble, France
e-mail: goulon@esrf.fr

I. Ogawa · T. Idehara
Research Center for the Development of Far Infrared Region,
University of Fukui (FIR-FU), Fukui-shi 910-8507, Japan

1 Magnetic resonance with element & edge selectivity

X-ray Detected Magnetic Resonance (XDMR) can be seen as a *Pump & Probe* experiment in which X-ray Magnetic Circular Dichroism (XMCD) is used to *probe* the resonant precession of either spin or orbital magnetization components in a strong *pump* field typically oscillating at microwave frequencies. It is the aim of this paper to discuss how far microwave pumping could be extended up to sub-THz frequencies. At this stage , this can only be envisaged for samples that are low-loss insulators, i.e. with no skin depth restriction. Regarding the penetration depth of X-rays, a critical distinction has anyhow to be made between "*soft*" and "*hard*" X-rays (E $<$ 2 keV .or. E $\geq$ 2 keV) since the beamline optics and instrumentation are fairly different for the two spectral ranges. Actually, XDMR experiments have been reported which used either hard-XMCD [1–5], or soft-XMCD [6–15]. In this paper, we shall concentrate on XDMR experiments to be performed at the X-ray absorption K-edges of magnetic 3d transition elements, i.e. in the 4.5–9.0 keV energy range.

As opposed to electron magnetic resonance (EMR) that can be pumped with poorly energetic photons ($E \leq 10$ cm^{-1}), XMCD refers to an atomic, core-level excitation process involving highly energetic photons with wave numbers in excess of 10^7 cm^{-1}. Typically, the life-time of X-ray excited states is considerably shorter than the time-scale of spin-orbit interactions and of collective magnetic excitations involving exchange and dipole-dipole interactions. XMCD thus delivers a *snapshot* picture of the precession dynamics of spin and orbital magnetization components in *excited states* in the immediate surrounding of a given X-ray absorbing atom: XDMR is then *element specific*, as opposed to ferromagnetic resonance (FMR).

Edge-selectivity of XDMR measurements is a further property linked to the conservation of angular momentum in the photoionisation process of deep atomic core levels, e.g. the 1s electrons of a K-shell or the 2p electrons of a L-shell. In the so-called *two-step* model [16], the angular momentum carried by a circularly polarized X-ray photon ($+\hbar$ for a right-handed circular polarization, $-\hbar$ for a left-handed circular polarization) is transferred to the excited photoelectron in a way that primarily depends on spin-orbit coupling in the excited core level. For $L_{2,3}$ absorption edges that are split by spin-orbit, the Fano effect implies that part of the photon angular momentum is converted into spin *via* spin-orbit coupling ($\ell + s$ at the L_3 edge; $\ell - s$ at the L_2 edge). No such conversion is possible at a K-edge (or L_1-edge) due to the absence of spin-orbit coupling in the core states and the photon angular momentum is entirely converted into $\pm\hbar$ orbital moments. The magnetic properties of the sample drive the second step: XMCD spectra simply reflect the difference in the density of final states that are allowed by the electric dipole ($E1$) or electric quadrupole ($E2$) selection rules owing to the symmetry of the initial core state. It immediately appears that an XMCD signal measured at a K-edge has to be definitely assigned to the *orbital* polarization of the valence band. The interpretation of the XMCD spectra recorded at spin-orbit split edges is more complicated since one has to disentangle the respective contributions of

spin and orbital polarizations. Summing all together the integrated dichroisms of electrons originating from conjugated sub-levels would again measure the orbital polarization of the final states; in contrast the *difference* in the integrated dichroic intensities measured at the spin-orbit split L_3 and L_2 edges can only be caused by a spin imbalance in the empty states because the orbital momentum transferred to the photoelectron has implicitly the same sign at both edges. This is essentially the physical content of what is known as the magneto-optical sum rules for XMCD [16].

In XDMR, it is most convenient to use a *differential* formulation of the XMCD sum rules as first proposed by Strange [17]. Restricting ourselves to electric dipole $E1$ transitions, one obtains at a K-edge [2, 5]:

$$[\Delta\sigma]_K = 3C_p \left\{ \frac{d}{dE} \langle L_z \rangle_p \right\}_{\Delta E} = 3C_p \langle \ell_z \rangle_p \tag{1}$$

in which $\Delta\sigma$ is the difference in the absorption cross-sections for left- and right-circularly polarized X-rays, $\Delta E = E_{\mathrm{RX}} + E_0 - E_F$ is the energy of the photoelectron referred to the Fermi level, C_p being a constant factor. Whereas $\langle L_z \rangle_p$ is the expectation value of the orbital magnetic moment integrated over all states featuring p-type symmetry, the effective operator $\langle \ell_z \rangle_p$ which appears in the right-hand side of Eq. 1 refers to the orbital polarization of p-projected densities of states (DOS). Taking into account electric quadrupole ($E2$) transitions will mix final states associated with atomic orbitals of different symmetry [2, 5]:

$$\langle \ell_z \rangle = \left\{ \langle \ell_z \rangle_{4p} + \epsilon \langle \ell_z \rangle_{3d} \right\} \tag{2}$$

Indeed, a similar break down may have to be considered if the final states need to be described with molecular orbitals, e.g. when the absorbing atom is in a tetrahedral ligand field. Anyhow, K-edge XDMR experiments refer to the forced precession of the energy-dependent *orbital magnetization* component $\langle \ell_z \rangle$.

XDMR cross-sections at $L_{2,3}$-edges can also be related to differential operators involving spin and orbital magnetization DOS [2]:

$$\begin{aligned} [\Delta\sigma]_{L_3} &= \frac{C_d}{3N_b} \frac{d}{d\Delta E} \left\{ \langle L_z \rangle_d + \frac{2}{3} \langle S_z \rangle_d + \frac{7}{3} \langle T_z \rangle_d \right\} \\ &= \frac{C_d}{3N_b} \left\{ \langle \ell_z \rangle_d + \frac{2}{3} \langle s_z \rangle_d + \frac{7}{3} \langle t_z \rangle_d \right\} \end{aligned} \tag{3}$$

$$\begin{aligned} [\Delta\sigma]_{L_2} &= \frac{C_d}{3N_b} \frac{d}{d\Delta E} \left\{ \langle L_z \rangle_d - \frac{4}{3} \langle S_z \rangle_d - \frac{14}{3} \langle T_z \rangle_d \right\} \\ &= \frac{C_d}{3N_b} \left\{ \langle \ell_z \rangle_d - \frac{4}{3} \langle s_z \rangle_d - \frac{14}{3} \langle t_z \rangle_d \right\} \end{aligned} \tag{4}$$

in which $N_b \simeq 2$ is the statistical branching ratio. Two distinct operators (s_z, t_z) are needed to describe the spin dynamics. Recall that $\langle t_z \rangle$ reflects (to

the lowest order) the asphericity of the spin magnetization due either to spin-orbit interactions or anisotropic charge distributions [16]. Fortunately, $\langle t_z \rangle_d / 2\langle s_z \rangle_d \ll 1$ in magnetic systems with cubic symmetry [5].

2 Precession dynamics of $\langle \ell_z \rangle$ & $\langle s_z \rangle$ up to THz pump frequencies

It has long been recognized that the torque equation: $\dot{\mathbf{J}} = \mathbf{M} \times \mathbf{H}$, which describes the precession of angular momenta, is only valid for free ions: it does not hold true in a crystalline environment as a consequence of spin-orbit interaction [18]. Similarly, the Hamiltonians describing exchange spin waves in solids most often ignore spin-orbit interactions whereas the phenomenological Landau–Lifshitz–Gilbert (LLG) or Bloembergen Bloch (BB) equations commonly used in FMR do work well when the spectroscopic splitting factor (g) is close to its free spin value ($g \simeq 2$) [5]. In other terms, there is -as yet- no microscopic theory that can rigorously describe the precession of the magnetization components associated with $\langle \ell_z \rangle$ or $\langle s_z \rangle$. It was nevertheless suggested elsewhere [2] that a formulation in terms of *local* LLG or BB equations could still be used as long as the resonance frequencies and linewidths measured by XDMR at a given absorbing edge are allowed to depart from the *effective* values measured with standard FMR. This is why it is desirable to carefully compare XDMR and FMR spectra recorded under identical pumping conditions [5].

In these recent years, high quality XDMR spectra have been recorded at the ESRF in the microwave X-band for a variety of ferrimagnetic iron garnet thin films [1–5]. For the first time, clear experimental evidence was produced that the forced precession of the *orbital* magnetization components $\langle \ell_z \rangle$ could be detected in YIG films at the iron K-edge [1]. The precession of spin-polarized magnetization components induced by charge delocalizations was also detected at the $L_{2,3}$ edges of ions such as Y^{3+} or La^{3+} which are most often given as "diamagnetic" [5]. Let us emphasize that the Fe K-edge XDMR spectra in YIG proved to be not only element-selective but *site* selective as well because the XMCD signal of the tetrahedral iron sites was shown to strongly dominate the very weak contribution of the ferrimagnetically coupled octahedral iron sites. Further XDMR work carried at the ESRF and which is still in progress concurred to demonstrate that, in YIG films, $\langle \ell_z \rangle$ could couple to magnetostatic spin waves through dipole-dipole interactions and to phonons through magneto-elastic interactions. Unsuspected collective excitations such as *orbitons* may also have to be taken into consideration [5].

Regarding ferrimagnets (and ultimately *antiferromagnets*), the scientific case of high-field XDMR experiments at sub-THz pumping frequency definitely deserves to be envisaged. One may dream to excite Kittel–Kaplan exchange modes in which antiferromagnetically coupled magnetization components would precess with opposite chirality and unequal opening cone angles [19]. Recent FMR studies at high pumping frequencies also pointed out that such measurements were helpful not only to refine the determination

of the spectroscopic splitting factor g [20], but also to unravel the hidden contribution of two-magnon relaxation processes if one carefully analyzes the frequency dependence of the FMR linewidths over a wide enough frequency range [21].

As of today, X-ray detected electron paramagnetic resonance (XDEPR) looks like an attractive challenge. Whereas the precession cone angles θ_0 are quite small in ferrimagnets, pulsed EPR spectrometers typically require the magnetization to be rotated by 90° or even 180° in the rotating frame [22–24]. Recall, however, that XMCD signals of paramagnetic phases were detected so far only under high magnetic bias fields ($B_0 \geq 5T$) and at fairly low temperatures ($T \leq 20K$): XDEPR spectra should thus be pumped at sub-THz frequencies [25]. For concentrated samples, there is an additional difficulty that the XDEPR lines could be rather broad if the exchange field (H_{ex}) does not largely exceed the dipolar field (H_{dd}) since, according to the Anderson–Weiss model for exchange narrowing, $\Delta H \propto H_{dd}^2/H_{ex}$ [26, 27]. XDEPR, nevertheless, could yield some unique information about the precession dynamics of *orbital* magnetization components in Van Vleck paramagnets that were proposed as polarizing agents for DNP applications [28]. One may also benefit from the well known advantages of high field EPR experiments: (i) EPR spectra can be measured in non-Kramers systems with integer spin and large zero-field splitting that are "EPR-silent" at microwave frequencies [29]; (ii) resonances affected by orientational anisotropy and hyperfine structures can be better resolved [24, 30].

3 Detection constraints for sub-THz XDMR

As illustrated with Fig. 1, there are two distinct configurations for an XDMR experiment:

– In the *transverse* geometry (TRD), the wavevector $\mathbf{k}_x$ of the incident, circularly polarized (CP) X-rays is set perpendicular to both the static bias

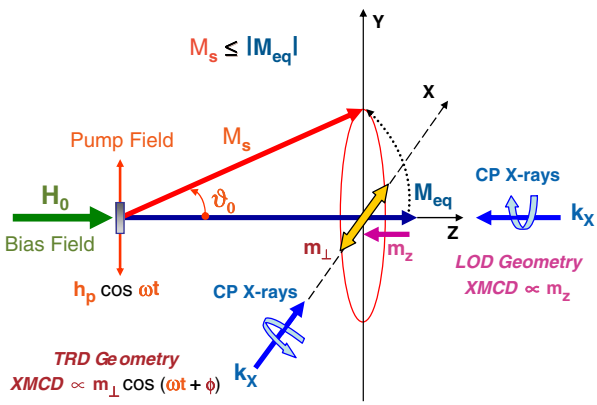

Fig. 1 XDMR in *TRD* and *LOD* geometries.

field $\mathbf{H}_0$ and the oscillating pump field $\mathbf{h}_p$: the XMCD probe signal is then proportional to the transverse magnetization $m_\perp$ which oscillates at sub-THz frequency.

– In the *longitudinal* geometry (LOD), the X-ray wavevector $\mathbf{k}_x$ is now set parallel to the static bias field $\mathbf{H}_0$. If one assumes that the equilibrium magnetization vector remains invariant in precession, i.e. $M_s = |\mathbf{M}_{\mathrm{eq}}|$, then there is a *steady-state* change m_z of the projection of the magnetization along the Z axis and there should be a time invariant XMCD signal $\propto m_z$. Unfortunately, m_z is only a 2nd order effect with respect to the opening angle of precession (θ_0) and $m_\perp$. Moreover, any information regarding the phase or the chirality of the precession gets lost.

For a ferromagnetic thin film with uniaxial anisotropy and perpendicular magnetization, the opening angle of precession θ_0 characterizes the precession dynamics: it can be determined by combining together XDMR and *static* XMCD cross-sections [2, 5]. For XDMR measurements in LOD geometry, one easily obtains:

$$\left[\Delta\sigma_{\mathrm{XDMR}}\left(k_\parallel\right)\right] / \left[\Delta\sigma_{\mathrm{XMCD}}\left(k_\parallel\right)\right] \simeq -1/2\tan^2\theta_0 \tag{5}$$

whereas in the TRD geometry:

$$\left[\Delta\sigma_{\mathrm{XDMR}}\left(k_\perp\right)\right] / \left[\Delta\sigma_{\mathrm{XMCD}}\left(k_\parallel\right)\right] \simeq \tan\theta_0 \sin\left[\omega t + \phi_0\right] \tag{6}$$

It should be stressed, however, that there is no X-ray detector that can measure a small dichroic signal oscillating at sub-THz nor at microwave frequencies. In the microwave X-band, high quality XDMR spectra could nevertheless be recorded using a heterodyne detection of the XMCD signal [3, 5]. This turned out to be possible by analyzing the consequences in the frequency domain of the time-structure of the excited X-ray fluorescence signal ($I_f(t)$) which consists of a series of discrete bunches, with a periodicity $\Delta T = 1/RF = 2.839$ ns defined by the RF frequency (352.202 MHz) of the storage ring. Let us admit that all bunches have a gaussian shape with a typical FWHM length of *ca.* 50 ps:

$$I_f(t) = I_{f_0} \sum_n \delta(t - n\Delta T) \otimes \frac{1}{\sigma\sqrt{2\pi}} \exp -\frac{t^2}{2\sigma^2} \tag{7}$$

On Fourier-transforming $I_f(t)$, one obtains in the frequency domain a Gaussian envelope of harmonics of the RF frequency:

$$H_f(F) = I_{f_0} RF \sum_n \delta(F - nRF) \exp -2(\pi\sigma F)^2 \tag{8}$$

At the ESRF, the half-width at half maximum of the gaussian envelope: $\Delta F_{1/2} \simeq 25 \times RF = 8.79$ GHz falls typically in the microwave X-band. In other terms, the ESRF storage ring directly provides us with a microwave local oscillator (LO) at a frequency close to the XDMR pumping frequency and it is much easier to detect the corresponding beating signal. Moreover, a substantial gain in sensitivity was obtained using a super-heterodyne detection scheme

which exploits a 180° bi-phase modulation technique (BPSK) [5]. Defining the XDMR pumping frequency as $F_p = N \times$ RF + IF, the superheterodyne detection consists in catching the modulation satellites at frequencies IF $\pm$ F_{bpsk}.

Unfortunately, there is no hope to extend the latter concept at sub-THz frequencies: this would require us to exploit RF harmonics of high order (e.g. N $\simeq$ 1,000 at 352 GHz) which are much weaker and unstable for practical use. This happens because, in high energy storage rings like the ESRF, the bunch length can hardly be reduced below 50 ps whereas this can be envisaged with 4th generation synchrotron radiation sources like X-ray free electron lasers (XFEL) or an energy recovering LINAC. Thus, at the ESRF, the only chance to extend XDMR up to sub-THz frequencies is to carry out the experiments in the LOD geometry which does not require any fast X-ray detector. The price to be paid will be a severe loss of sensitivity since we are looking for a 2nd order effect.

In previous XDMR experiments performed in LOD geometry [1–5], the microwave pumping power was amplitude modulated (AM) at low frequency. We significantly improved the immunity against artefacts by exploiting the *macrobunch* time-structure in the storage ring which causes the incident X-ray beam and the detected X-ray fluorescence signal to be both modulated at frequency $F_{RX} = n \times F_0$, in which F_0 denotes the revolution frequency of the electron bunches in the storage ring, i.e. F_0 = RF/992 = 355.0427 kHz and n is the relevant harmonic order. Such a modulation of the X-ray beam intensity arises when the 992 relativistic electron bunches circulating in the storage ring are only partially filled: typically, the 7/8 filling mode which favours the lowest harmonics ($n = 1$) has now become a standard operation mode of the ESRF storage ring. The XDMR signal should then show up as modulation sidebands at $F = F_{RX} \pm F_{AM}$.

As an illustrative example, we have reproduced in Fig. 2 a typical display of the vector Spectrum Analyzer (VSA: Agilent Technologies Inc. 89600-SU) operated in the *time-averaged* mode using a synchronous low frequency

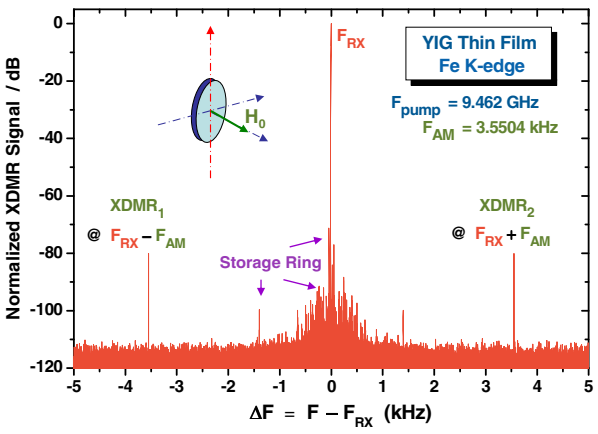

Fig. 2 Typical VSA display showing the XDMR modulation sidebands. The experiment carried in LOD geometry was performed at the Fe *K*-edge using a thin film of YIG deposited on a GGG substrate. The corresponding pumping power was *ca* 28 dBm (650 mW) in the microwave X-band.

triggering reference ($F_{tg} = F_m/q$). In this experiment, the X-ray fluorescence detector was a large area X-ray photodiode associated with a home-made preamplifier/readout electronics [31]. It clearly appears from Fig. 2 that the XDMR signatures measured in LOD geometry are very weak and their measurement requires from the whole detector readout electronics a dynamic range in excess of 110 dB. Actually, XDMR experiments carried out at sub-THz frequencies are much more demanding from the detector electronics because the precession cone angle θ_0 decreases when increasing the pumping frequency so that the XDMR signal vanishes as: $\Delta\sigma \propto P_p/\omega^2$, in which P_p denotes the effective pumping power and ω the precession frequency. Thus, if one would preserve the same effective pumping power, one should anticipate a loss of sensitivity amounting to 18 dB at 76 GHz, 23 dB at 138 GHz or 31 dB at 354 GHz. Increasing the effective pumping power is thus mandatory for a successful XDMR experiment at sub-THz frequencies.

4 XDMR using a high power gyrotron source

Whereas the current technology for sub-THz semiconductor amplifiers is restricted to rather low output powers ($P_1 \leq 100$ mW), gyrodevices can deliver up to kW peak power in pulsed mode operation and look like attractive sources for XDMR experiments up to THz frequencies.

Compared to other high power sources such as extended interaction klystrons or TWT, gyrotrons benefit of the major advantage that the frequency is step-tunable [32, 33]. From earlier work carried out at the FIR-FU center over several decades, it is well documented that proper conditions for either fundamental ($s = 1$) or second harmonic ($s = 2$) electron cyclotron resonance can be realized for several cavity modes by carefully adjusting the external magnetic field [34]. This is illustrated with Fig. 3 which reproduces the field

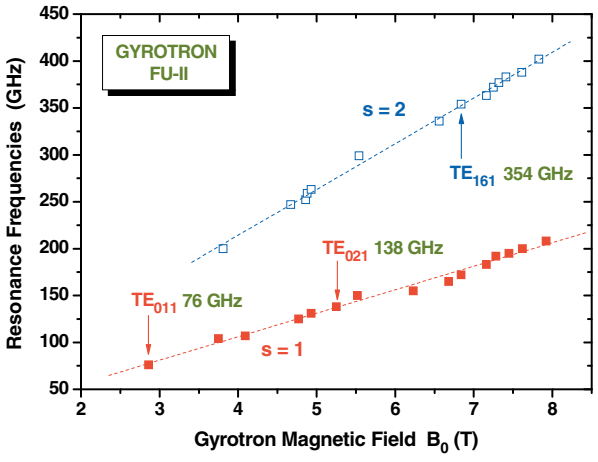

Fig. 3 Field dependence of the emission frequencies of gyrotron FU-II associated with different cavity modes under the conditions of fundamental ($s = 1$) or first harmonic ($s = 2$) electron cyclotron resonance [34]. *Arrows* refer to specific modes which were previously used to deliver high output intensities with peak power ≥1 kW.

dependence of the observed emission frequencies of gyrotron FU-II that was used for the test experiments reported in this paper. Using short pulses of 100 μs duration at 5 Hz repetition rate, the output peak powers of gyrotron FU-II were as high as 5.4 kW in the TE_{011} mode, and 0.9 kW in the TE_{161} mode. With a more recent design (e.g. gyrotron FU CW V) optimized for continuous wave (cw) operation, typical cw output powers of 180 and 20 W were measured at 77 and 360 GHz respectively. Such figures look very encouraging for XDMR experiments even though the long term stability of the gyrotron radiation may be poor, especially for high output powers [35]. We also experienced some restrictions regarding the amplitude modulation frequencies using an external generator synchronously driven by the ESRF reference clock.

A priori, it should not be taken for granted that the XDMR signal measured in LOD geometry will systematically grow on increasing the pumping power [2]. Due to the strongly *non-linear* character of the LLG equation, it is well documented that the FMR lineshape undergoes strong distortions under high pumping power: this is commonly known as the *foldover* effect [19]. Its origin can be found in the fact that, in ferrimagnetic films featuring a large magnetic anisotropy, the resonance condition depends explicitly on the precession cone angle θ_0, which itself depends implicitly on the circularly polarized pump field h_{pump}. As illustrated with Fig. 4, the equation yielding θ_0 becomes multivalued at high pumping power and field swept spectra clearly exhibit an hysteretic character [2].

Whereas foldover effects are quite dramatic in the microwave X-band or at lower frequencies, it is encouraging to observe that the latter distortions become marginal in the sub-THz range, at least for YIG films, even if the

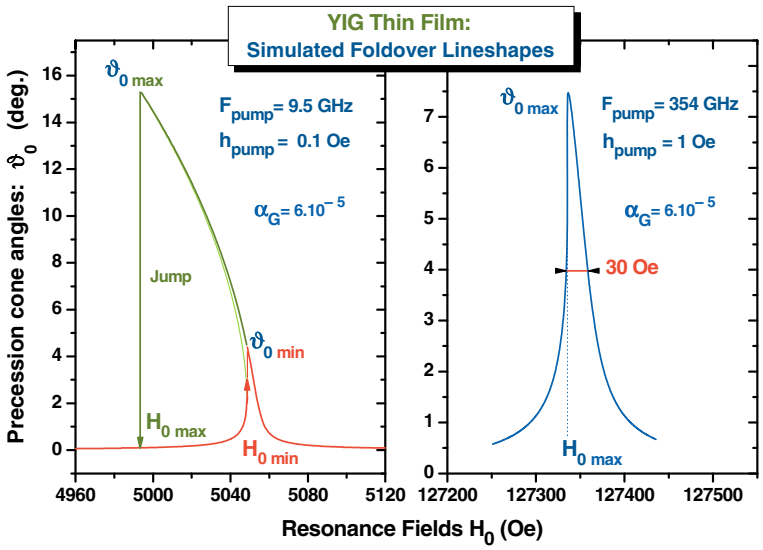

Fig. 4 Simulated lineshapes in the foldover regime for a perpendicularly magnetized YIG thin film; **a** CW Pumping in the microwave *X*-band at 9.5 GHz; **b** at 354 GHz.

pumping power is increased by two orders of magnitude: this is due to the fact that the internal anisotropy field becomes much smaller than the bias field H_0 whereas the resonance linewidth increases linearly with frequency for a constant Gilbert damping factor ($\alpha_G \simeq 6 \times 10^{-5}$). The simulations reproduced in Fig. 4, however, neglected another difficulty: a saturation of the precession cone angle is to be expected when the microwave pump field exceeds some critical threshold field hth beyond which the uniform precession mode ($k = 0$) couples to degenerate spin waves ($k \neq 0$). In the late fifties [36], Suhl identified two non-linear processes by which uniform magnons could be destroyed and pointed out that the relevant instability thresholds could be raised on modulating either the pump frequency or the bias field [37]. Note that the first order instability process -which contributes to a so-called *subsidiary* absorption in FMR- becomes inactive for a perpendicularly magnetized sample: this is precisely the configuration which will be retained for the experiments discussed in the next section.

5 Test experiments at the ESRF

The ESRF and the FIR-FU teams agreed to join their own expertises in order to carry out together a series of feasibility test experiments using a mm-wave XDMR spectrometer installed on the ESRF beamline ID12 and which exploits the gyrotron FU-II as a high power pumping source. Recall that beamline ID12 is the only beamline world-wide that is entirely dedicated to X-ray circular or linear dichroism studies over the whole energy range 2–20 keV. It is equipped with three helical undulator sources that can deliver very high fluxes of circularly polarized X-ray photons [38, 39]. As a key part of this project, the 20 year-old gyrotron FU-II was carefully refurbished in Fukui before it was shipped to the ESRF. It is currently installed in the 4th experimental hutch of beamline ID12, its operation being remotely controlled when the X-ray beam is switched on. It was decided to concentrate first on FMR and XDMR experiments performed at 76 and 138 GHz, i.e. on operating the gyrotron at the fundamental resonances of the TE_{011} and TE_{021} modes. FMR & XDMR experiments were conducted in a split coil cryomagnet (Magnex Scientific Inc., Yarnton-Oxford, U.K.) under a magnetic bias field $\mathbf{H_0} \leq 6$T oriented parallel to the X-ray wavevector. Building on earlier experience gained at the ESRF from XDMR studies of iron garnet films, YIG or Gadolinium doped YIG films deposited on GGG substrates were selected as good candidates for the proposed test experiments.

5.1 Modular quasi-optical FMR spectrometer

Owing to the high level of stray field induced by the 6T split coil magnet, it was desirable to keep the gyrotron FU-II distant from the XDMR spectrometer: typically, a 4m long transfer line connected the gyrotron FU-II to the ESRF mm-wave spectrometer operated in the quasi-optical mode. Rather than using

corrugated waveguides for low transmission losses, we found it preferable to use a circular waveguide of large inner diameter ($Ø = 52$ mm) in order to approach the conditions of plane-wave propagation at 76 GHz with $(\lambda_g - \lambda)/\lambda \leq 0.005$ in all modes, λ_g and λ denoting the wavelengths of the guided and (optical) free waves respectively. The modular spectrometer sketched in Fig. 5a included a Quasi-Optical Michelson interferometer combining a fused Quartz beam splitter and two sliding mirrors. A second module was added to monitor the gyrotron radiation intensity. Planoconvex dielectric lenses, machined from teflon, allowed us to refocus the whole pumping power onto the sample, at least within the diffraction limits. The sample holder, introduced through a lateral port of the split coil magnet, can be rotated in order to vary the polar angle $(90° - \beta)$ of the normal to the probed film with respect to the direction of the magnetic bias field $\mathbf{B_0}$.

FMR spectra were measured in transmission mode using a commercially available pyroelectric detector connected to a lockin amplifier given that the power radiated by gyrotron FU-II was square modulated at $F_{AM} = F_0/1{,}300 = 273$ Hz with a duty cycle of *ca.* 10%. Typical spectra recorded at 76 and 137 GHz are reproduced in Fig. 5b in which we removed the broad background

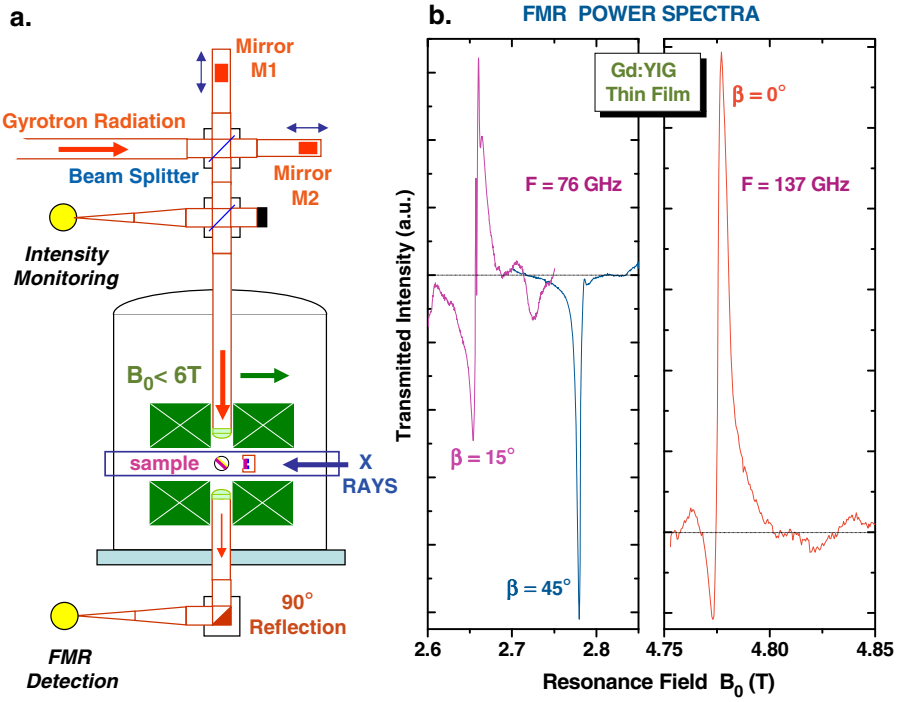

Fig. 5 **a** Quasi-Optical spectrometer based on a Michelson interferometer built in circular oversized waveguide ($Ø = 52$ mm) and refocusing lenses ; **b** FMR spectra recorded in transmission mode at 76 and 137 GHz using Gyrotron FU-II as pumping source; $\beta = 0°$ refers to in-plane magnetization and $\beta = 90°$ for perpendicular magnetization.

absorption due to the paramagnetic GGG substrate of the Gd:YIG film grown by liquid phase epitaxy. Note that the simple detection scheme used here did not allow us to discriminate between the dispersive (χ') and absorptive (χ'') parts of the resonance spectra which clearly tend to mix together when the sample is rotated since the GGG substrate tends to act as a *phase plate* of variable thickness.

Unfortunately, any attempt to record a small XDMR signal in this configuration failed. The primary cause for this failure is that the XDMR signal which we were looking for was dramatically masked by a huge parasitic signal at the detection frequency: $F_0 \pm F_{AM}$. This parasitic signal was partly due to a modulation of the ground plane of the X-ray detector when the gyrotron is operated at high radiation power. A direct detection of the mm-waves may also be possible if the bonding wires of the photodiode act as unwanted sub-THz detection antennas. Given that the level of the parasitic signal was at least 60 dB above the level of the expected XDMR signal, it became clear that dramatic changes in the detection concept were mandatory.

5.2 XDMR in frequency-mixing mode

The latter test experiments confirmed our suspicion that amplitude modulation was not a suitable option at high pumping power. Frequency modulation is a promising alternative which deserves to be explored since it may be the only way to detect a weak XDMR signal at 354 GHz or even higher frequencies. Pioneering work done at the FIR-FU proved that the frequency of the gyrotron radiation could be modulated with an amplitude of several tens of MHz in modulating the gyrotron cavity body voltage [40, 41]. Unfortunately, this option can only be implemented with gyrotrons of recent generation and cannot be performed with gyrotron FU-II.

In this section, we like to draw attention onto a totally new approach which would be fully compatible with the operation of gyrotron FU-II operated at 76 or 138 GHz where the radiation intensity is very high. This approach, which exploits the non-linearity of XDMR in LOD geometry, is based on the well established concept of frequency mixing by a ferromagnetic sample at resonance [19]. If the sample is pumped at two discrete frequencies: $\boldsymbol{\omega}^{(1)}$ and $\boldsymbol{\omega}^{(2)} = \boldsymbol{\omega}^{(1)} + \Delta\boldsymbol{\omega}$, where $\Delta\boldsymbol{\omega}$ is kept well below the FMR linewidth, then the XDMR signal will result from three contributions: $m_z^{(1)} + m_z^{(2)} + m_z^{(1,2)} \times \cos(\Delta\boldsymbol{\omega} \cdot t + \phi)$. Whereas the first two terms are the steady-state contributions expected for each individual pumping frequency, the third term is now oscillating at the beating frequency $\boldsymbol{\omega}^{(2)} - \boldsymbol{\omega}^{(1)}$ with: $m_z^{(1,2)} \propto [h_{cp}^{(1)} \cdot h_{cp}^{(2)}]/(\boldsymbol{\omega}_0)^2$ in which $h_{cp}^{(j)}$ denotes the effective (circularly polarized) pump field at frequency $\boldsymbol{\omega}^{(j)}$ whereas $\boldsymbol{\omega}_0$ is the resonance frequency in the external bias field $\mathbf{B_0}$. The proposed challenge is to detect the beating term which causes the frequency mixing effect.

A practical realization of this concept at 76 GHz is illustrated with Fig. 6. Whereas $\boldsymbol{\omega}^{(1)}$ refers to the frequency of the intense gyrotron radiation, the

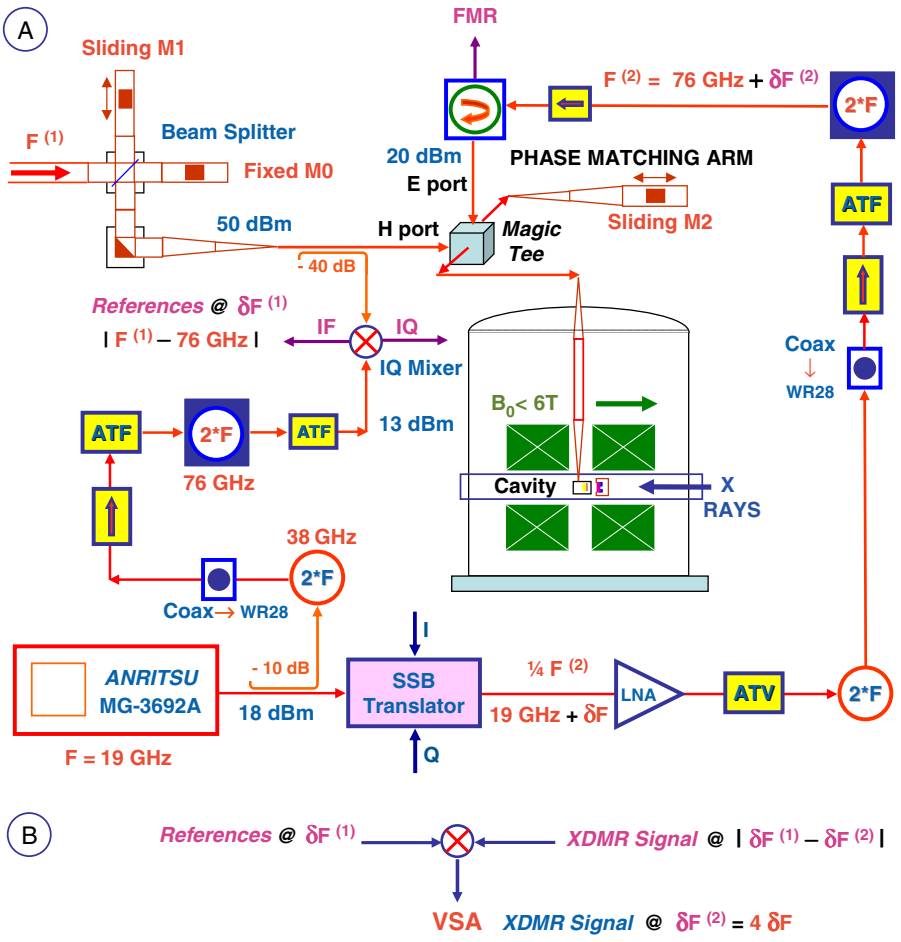

Fig. 6 **a** XDMR in frequency mixing mode: the sample mixes the intense gyrotron radiation at frequency $F^{(1)} = 76$ GHz $+\delta F^{(1)}$ with an ultra stable reference at frequency $F^{(2)} = 76$ GHz $+\delta F^{(2)}$. **b** The XDMR signal can be down-converted to frequency $\delta F^{(2)}$ if the beating signal measured at frequency ΔF is mixed in real time with the outputs of the I/Q mixer.

radiation at frequency $\omega^{(2)}$ is generated from a tunable microwave generator (Anritsu) operated at 19 GHz using two cascaded (active) frequency doublers. One may increase the detection sensitivity using again a superheterodyne detection of the weak XDMR signal. In this perspective, $\Delta\omega$ is split into two contributions: $\delta\omega^{(1)} + \delta\omega^{(2)}$. Whereas $\delta\omega^{(1)}$ -which includes the undesired drifts of the gyrotron frequency- is measured in real time using a E-band I/Q mixer, a fully controlled frequency shift $\delta\omega^{(2)}$ is produced by a microwave single side-band (SSB) translator driven by synchronous signals (I and Q) that are sub-harmonics of the ultastable RF reference of the ESRF storage ring. A very high level of immunity against artefacts can be reached in detecting the XDMR component oscillating at $\delta\omega^{(2)}$. This is possible if the output signal of

the photodiode at frequency $\Delta\omega$ is preamplified and mixed with the IF/IQ references measured at frequency $\delta\omega^{(1)}$ in order to translate the frequency of the XDMR signal by $-\delta\omega^{(1)}$.

The safe combination of the two pumping intensities at frequency $\omega^{(1)}$ and $\omega^{(2)}$ is not a trivial task: it is realized in a E-band matched hybrid tee (magic tee) that benefits from an isolation as high as 30 dB between the E- and H-ports. Carefully cooled ferrite circulators/isolator do also help us to reach the very high level of isolation that is ultimately desired.

The price to be paid for a better immunity against artefacts is a severe loss in sensitivity because $m_z^{(1,2)} \propto [P^{(1)} \cdot P^{(2)}]^{1/2} \ll P^{(1)}$. We tried to minimize it by inserting the sample in a TE_{0mn} cylindrical cavity [42] optimized for XDMR experiments at 76 or 138 GHz. Attention was paid to the following points: (i) the incident X-ray beam should enter the cavity without creating any leak of sub-THz radiation that would perturb the X-ray detector; (ii) the X-ray beam should be absorbed in the YIG film -not in the GGG substrate nor any absorbing window material-; (iii) the solid angle over which the excited fluorescence X-ray photons are collected outside the cavity should be maximized. As illustrated with Fig. 7, we found it also preferable to rigidly assemble together the sub-THz cavity and the X-ray detector.

The cavity volume is split into two sections: (i) the coupling one ($\varnothing_c = 9.438$ mm; $L_c \simeq 10.898$ mm) is empty and allows us to adjust the resonance frequency of the selected TE_{02n} mode; (ii) the second one ($\varnothing_d = 9.838$ mm; d $= 1.20$ mm) is entirely filled with a sapphire disk in which the small sample ($\varnothing_s = 1.5$ mm; e $\simeq 0.457$ mm) is incrusted. Note that the electric permittivity of the GGG substrate ($\varepsilon_r \simeq 12.1$) is comparable to that of sapphire ($\varepsilon_r \simeq 11.6$). With its excellent thermal conductivity and negligible dielectric losses, the sapphire disk prevents the sample from being damaged over long data acquisition times at high pumping power. The YIG thin film is directly in contact with a thin Beryllium (Be) disk (0.025 mm thick) acting as an X-ray transparent metallic short circuit. A second Be window was inserted to enhance the protection of the X-ray photodiode.

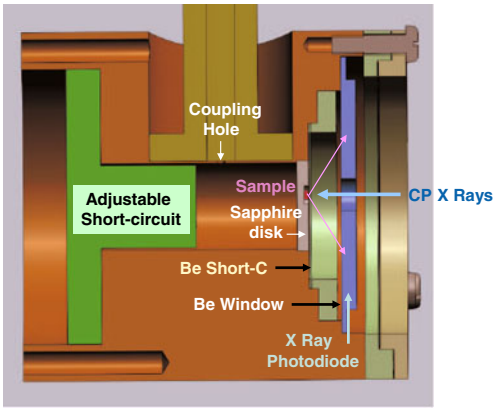

Fig. 7 X-ray detector and TE_{02n} cylindrical cavity for XDMR experiments at 76 GHz.

Obviously, $\boldsymbol{\omega}^{(1)}$ and $\boldsymbol{\omega}^{(2)}$ should be adjusted close enough to the resonance frequency of the cavity ($\boldsymbol{\omega}_{\mathrm{cav}}$). This condition can be easily satisfied for $\boldsymbol{\omega}^{(2)}$ by tuning the frequency of the Anritsu microwave generator. It is not so easy to adjust $\boldsymbol{\omega}^{(1)}$ near $\boldsymbol{\omega}_0$ and $\boldsymbol{\omega}_{\mathrm{cav}}$, e.g. within the FMR linewidth ($\Delta F = 175$ MHz for the Gd:YIG film). One way to do this, is to use the *frequency pulling* technique [43] which consists in slightly varying the magnetic field driving the gyrotron electron cyclotron resonance. This point still deserves further tests with gyrotron FU-II.

6 Conclusion

At this stage, we are fully confident that XDMR measurements can readily be extended at the ESRF up to 140 GHz with gyrotron FU-II. Any further extension (e.g. up to 354 GHz), would definitely require a careful optimization of the gyrotron source and the design of a quasi-optical resonator. We like to stress, however, that XDMR is a *unique tool* to probe the precession dynamics of *orbital* magnetization components at a precession time scale that is considerably shorter than the duration of the relativistic electron bunches in the ESRF storage ring. So-far, there is no other example of such ultrafast process probed with hard X-rays at a 3rd generation synchrotron radiation source. It still remains to be proven that synchrotron radiation sources of 4th generation (XFELs, Energy recovering LINACs) will ever benefit of the ultra high sensitivity and of the excellent stability required to extend such experiments at sub-ps time scales, given that the precession cone angle θ_0 decreases linearly with frequency.

Acknowledgements Invaluable technical assistance by M.-C. Dominguez, S. Feite and P. Voisin are warmly acknowledged here. Nothing would have been possible without the support and encouragements of F. Sette.

References

1. J. Goulon, A. Rogalev, F. Wilhelm, N. Jaouen, Ch. Goulon-Ginet, G. Goujon, J. Ben Youssef, M.V. Indenbom, *X-ray detected magnetic resonance at the Fe K-edge in YIG: forced precession of orbital magnetization components*. JETP Lett. **82** (2005), 791–795.
2. J. Goulon, A. Rogalev, F. Wilhelm, N. Jaouen, Ch. Goulon-Ginet, Ch. Brouder, *X-ray detected ferromagnetic resonance in thin films*. Eur. Phys. J. B **53** (2006), 169–184.
3. J. Goulon, A. Rogalev, F. Wilhelm, Ch. Goulon-Ginet, G. Goujon, *Element-selective X-ray detected magnetic resonance in thin films*. J. Synchrotron Rad. **14** (2007), 257–271.
4. J. Goulon, A. Rogalev, F. Wilhelm, G. Goujon, *X-ray Detected Magnetic Resonance*, in: *Magnetism and Synchrotron Radiation*, Springer Proc. in Phys., **133**, E. Beaurepaire, H. Bulou, F. Scheurer, J.-P. Kappler Eds. (Springer-Verlag: Berlin-Heidelberg, 2010), pp. 191–222.
5. J. Goulon, A. Rogalev, F. Wilhelm, G. Goujon, Ch. Brouder, A. Yaresko, J. Ben Youssef, M.V. Indenbom, *X-ray detected magnetic resonance of YIG thin films in the non-linear regime of spin waves*. J. Magn. Magn. Mater. **322** (2010), 2308–2329.
6. W.E. Bailey, L. Cheng, D.J. Keavney, C.-C. Kao, E. Vescovo, D.A. Arena, *Precessional dynamics of elemental moments in a ferromagnetic alloy*. Phys. Rev. B **70** (2004), 172403(1–4).

7. D.A. Arena, E. Vescovo, C.-C. Kao, Y. Guan, W.E. Bailey, *Weakly coupled motion of individual layers in ferromagnetic resonance*, Phys. Rev. B **74** (2006), 064409(1–7).
8. D.A. Arena, E. Vescovo, C.-C. Kao, Y. Guan, W.E. Bailey, *Combined time-resolved x-ray magnetic circular dichroism and ferromanetic resonance studies of magnetic alloys and multilayers*. J. Appl. Phys. **101** (2007), 09C109(1–6).
9. Y. Guan, W.E. Bailey, E. Vescovo, C.-C. Kao, D.A. Arena, *Phase and Amplitude of element-specific moment precession in* $Ni_{81}Fe_{19}$. J. Mag. Magn. Mater. **312** (2007), 374–378.
10. D.A. Arena, Y. Ding, E. Vescovo, S. Zohar, Y. Guan, W.E. Bailey, *A compact apparatus for studies of element and phase-resolved ferromagnetic resonance*. Rev. Sci. Instrum. **80** (2009), 083903–083907.
11. G. Boero, S. Rusponi, P. Bencock, R.S. Popovic, H. Brune, P. Gambardella, *X-ray ferromagnetic resonance spectroscopy*. Appl. Phys. Lett. **87** (2005), 152503(1–3).
12. G. Boero, S. Mouaziz, S. Rusponi, P. Bencok, F. Nolting, S. Stepanow, P. Gambardella, *Element-resolved x-ray ferrimagnetic and ferromagnetic resonance spectroscopy*. New J. Phys. **10** (2008), 013011(1–12).
13. G. Boero, S. Rusponi, P. Bencok, R. Meckenstock, J.-U. Thiele, F. Nolting, P. Gambardella, *Double-resonant x-ray and microwave absorption: atomic spectroscopy and precessional orbital and spin dynamics*. Phys. Rev. B **79** (2009), 224425(1–8).
14. G. Boero, S. Rusponi, J. Kavich, A. Lodi Rizzini, C. Piamonteze, F. Nolting, C. Tieg, J.-U. Thiele, P. Gambardella, *Longitudinal detection of ferromagnetic resonance using transmission measurements*. Rev. Sci. Instrum. **80** (2009), 123902(1–11).
15. M.K. Marcham, P.S. Keatley, A. Neudert, R.J. Hicken, S.A. Cavill, L.R. Shelford, G. van der Laan, N.D. Telling, J.R. Childress, J.A. Katine,P. Shafer, E. Arenholz, *Phase-resolved x-ray ferromagnetic resonance measurements in fluorescence yield*. J. Appl. Phys. **109** (2011), 07D353(1–3).
16. A. Rogalev, F. Wilhelm, N. Jaouen, J. Goulon, J.-P. Kappler, *X-ray Magnetic Circular Dichroism: Historical Perspective and Recent Highlights*, in: *Magnetism: A Synchrotron Radiation Approach*, Lect. Notes in Phys., **697**, E. Beaurepaire, H. Bulou, F. Scheurer, J.-P. Kappler Eds. (Springer-Verlag: Berlin-Heidelberg, 2006), pp. 71–94.
17. P. Strange, *Magnetic absorption and sumrules in itinerant magnets*. J. Phys.: Condens. Matter **6** (1994), L491–L495.
18. M. Blume, G. Geschwind, A. Yafet, *Generalized Kittel–Van Vleck Relation between g and g′: validity for Negative g Factors*. Phys. Rev. **181** (1969), 478–487.
19. A.G. Gurevich, G.A. Melkov: *Magnetization Oscillations and Waves* (CRC Press Inc., Boca Raton, 1996).
20. R. Karim, K.D. McKinstry, J.R. Truedson, C.E. Patton, *Frequency dependence of the FMR linewidth in single crystal Barium ferrite platelets*. IEEE Trans. Magn. **28** (1992), 3225–3227.
21. K. Lenz, H. Wende, W. Kuch, K. Baberschke, K. Nagy, A. Jànossy, *Two-magnon scattering and viscous Gilbert damping in ultrathin ferromagnets*. Phys. Rev. B **73** (2006), 144424(1–6).
22. M.K. Bowman, *Fourier Transform Electron Spin Resonance*, in: *Modern Pulsed and Continuous-Wave Electron Spin Resonance*, L. Kevan, M.K. Bowman Eds. (John Wiley & Sons Inc., New York, 1990), pp. 1–42.
23. G.W. Morley, L.-C. Brunel, J. van Tol, *A multifrequency high field pulsed electron paramagnetic resonance/electron-nuclear double resonance spectrometer*. Rev. Sci. Instrum. **79** (2008), 064703(1–5).
24. A. Savitsky, K. Möbius, *High Field EPR*. Photosynth. Res. **102** (2009), 311–333.
25. J. Goulon, A. Rogalev, F. Wilhelm, G. Goujon, T. Idehara, *Sub-THz Gyrotron Optimized for X-ray Detected Electron Magnetic Resonance*. J. Plasma Fusion Res. **84** (2008), 909–911.
26. P.W. Anderson, P.R. Weiss, *Exchange Narrowing in Paramagnetic Resonance*. Rev. Mod. Phys. **25** (1953), 269–276.
27. B. Cage, P. Cevc, R. Blinc, L.-C. Brunel, N.S. Dalal, *EPR linewidths for* K_3CrO_8*: a comprehensive test for the Anderson-Weiss Model*. J. Magn. Reson. **135** (1998), 178–184.
28. D.A. Tayurski, M.S. Tagirov, H. Suzuki, *Investigations of dielectric Van Vleck paramagnets at high magnetic fields and low temperatures*. Physica B **284–288** (2000), 1686–1687.
29. J. Krzystek, A. Ozarowski, J. Telser, *Multi-frequency, high-field EPR as a powerful tool to accurately determine zero-field splittings in high-spin transition metal coordination complexes*. Coordin. Chem. Rev. **250** (2006), 2308–2324.

30. G.M. Smith, P.C. Riedi, *Progress in High Field EPR*, in: *Electron Paramagnetic Resonance*, RSC specialist periodical report (The Royal Society of Chemistry (RSC), Cambridge, U.K.) **17** (2000), chapt. 6, 164–204.
31. J. Goulon, A. Rogalev, G. Goujon, Ch. Gauthier, E. Moguiline, A. Solé, S. Feite, F. Wilhelm, N. Jaouen, Ch. Goulon-Ginet, P. Dressler, P. Rohr, M.-O. Lampert, R. Henck, *Advanced detection systems for x-ray fluorescence excitation spectroscopy*. J. Synchrotron Rad. **12** (2005), 57–69.
32. V. Bratman, M. Glyavin, T. Idehara, Yu. Kalynov, A. Luchinin, V. Manuilov, S. Mitsudo, I. Ogawa, T. Saito, Y. Tatematsu, V. Zapevalov, *Review of Subterahertz and Terahertz Gyrodevices at IAP RAS and FIR FU*. IEEE Trans. Plasma Sci. **37** (2009), 36–43.
33. S.P. Sabchevski, T. Idehara, *Design of a Compact Sub-Terahertz Gyrotron for Spectroscopic Applications*. J. Infrared Milli. Terahz. Waves **31** (2010), 934–948.
34. T. Idehara, T. Tatsukawa, I. Ogawa, H. Tanabe, T. Mori, S. Wada, G.F. Brand, M.H. Brennan, *Development of a second cyclotron harmonic gyrotron operating at submillimeter wavelengths*. Phys. Fluids B **4** (1992), 267–273.
35. I. Ogawa, T. Idehara, M.Ui, S. Mitsudo, W. Förster, *Stabilization and modulation of the output power of a submillimeter wave gyrotron*. Fusion Engin. & Design **53** (2001), 571–576.
36. H. Suhl, *Note on the saturation of the main resonance in ferromagnetics*. J. Appl. Phys. **30** (1959), 1961–1964; *Foldover effects caused by spin wave interactions in FMR*. J. Appl. Phys. **31** (1960), 935–936.
37. H. Suhl, *Restoration of stability in ferromagnetic resonance*. Phys. Rev. Lett. **6** (1961), 174–176.
38. J. Goulon, A. Rogalev, Ch. Gauthier, Ch. Goulon-Ginet, S. Pasté, R. Signorato, C. Neumann, L. Varga, C. Malgrange, *Instrumentation Developments for X-ray Linear and Circular Dichroism at the ESRF Beamline ID12A*. J. Synchrotron Rad. **5** (1998), 232–238.
39. A. Rogalev, J. Goulon, Ch. Goulon-Ginet, C. Malgrange, *Instrumentation developments for polarization dependent X-ray spectroscopies at the ESRF beamline ID12*, in: *Magnetism and Synchrotron Radiation Approach*, Lect. Notes in Phys., **565**, E. Beaurepaire, F. Scheurer, G. Krill, J.-P. Kappler Eds. (Springer-Verlag Berlin Heidelberg, 2001), pp. 60–86.
40. T. Idehara, M Pereyaslavets, N. Nishida, K. Yoshida, I. Ogawa, *Frequency Modulation in a Submillimeter-Wave Gyrotron*. Phys. Rev. Lett. **81** (1998), 1973–1976.
41. M Pereyaslavets, T. Idehara, N. Nishida, K. Yoshida, I. Ogawa, *Simulation and measurement of frequency modulation in submillimeter wave gyrotron*. IEEE Trans. Plasma Sci. **27** (1999), 363–367.
42. M. Mola, S. Hill, Ph. Goy, M. Gross, *Instrumentation for millimeter-wave magnetoelectrodynamic investigations of low dimensional conductors and superconductors*. Rev. Sci. Instrum. **71** (2000), 186–200.
43. T. Kariya,T. Saito, Y. Kiwamoto, H. Gotoh, S. Miyoshi, *Observation of Frequency Pulling Effect in Gyrotron*. Jpn. J. Appl. Phys. **25** (1986), 654–655.